ChemPhysChem

Research Article
doi.org/10.1002/cphc.202200060

Chemistry Europe
European Chemical Societies Publishing

www.chemphyschem.org

Ligand-Induced Tuning of the Electronic Structure of Rhombus Tetraboron Cluster

Ya Zhao[+],[a, b] Tiantong Wang[+],[b, e] Chong Wang[+],[b, e] Zhaoyan Zhang[+],[b, e] Huijun Zheng,[b, e] Shuai Jiang,[a, b] Wenhui Yan,[b, e] Hua Xie,[b] Gang Li,*[b] Jiayue Yang,[b] Guorong Wu,[b] Weiqing Zhang,[b] Dongxu Dai,[b] Xiucheng Zheng,*[a] Hongjun Fan,*[b] Ling Jiang,*[b] Xueming Yang,[b, d] and Mingfei Zhou*[c]

A neutral boron carbonyl complex $B_4(CO)_3$ is generated in the gas phase and is characterized by infrared plus vacuum ultraviolet (IR + VUV) two-color ionization spectroscopy and quantum chemical calculations. The complex is identified to have a planar C_{2v} structure with three CO ligands terminally coordinated to a rhombus B_4 core. It has a closed-shell singlet ground state that correlates to an excited state of B_4. Bonding analyses on $B_4(CO)_3$ as well as the previously reported B_4 and $B_4(CO)_2$ indicate that the electronic structure of rhombus tetraboron cluster changes from a close-shell singlet to an open-shell singlet in $B_4(CO)_2$ and to a close-shell singlet in $B_4(CO)_3$, demonstrating that the electronic structures of boron clusters can be effectively tuned via sequential CO ligand coordination.

Introduction

The electronic structures play an essential role in the determination of various physical and chemical properties of molecular systems.[1–6] Low-band gap compounds such as polycyclic hydrocarbons with closed-shell and open-shell states have shown their potential applications to the dye chemistry, nonlinear optics, and energy storage devices.[7] A series of non-Kekule molecules with tunable singlet-triplet energy spacings have also been synthesized.[8] Recent investigations have shown that boron-based molecules exhibit unique electronic structures due to the electron deficiency of boron and mimic the bonding properties and reactivity of transition-metal complexes.[9–12]

CO is an important ligand for the efficient tuning of electronic structures of metal clusters that are important in many heterogeneous and homogeneous catalytic processes, such as Fischer-Tropsch chemistry, hydroformylation, and acetic acid synthesis.[13–16] The diatomic B_2 molecule is a single bonded species with a triplet electronic ground state in $(1\sigma_g)^2(1\sigma_u)^2(2\sigma_g)^2(2\sigma_u)^2(1\pi_x)^1(1\pi_y)^1$ configuration, in which two valence electrons are in the σ bonding orbital ($2\sigma_g$), two valence electrons are in the σ antibonding orbital ($2\sigma_u$), and two unpaired electrons are in the two degenerate π bonding orbitals ($1\pi_x$ and $1\pi_y$), respectively.[17] Upon coordination of two CO ligands, the OCBBCO complex was determined to have a closed-shell singlet ground state that correlates to an excited state B_2 with B≡B triple bonding.[18] Binding of two CO ligands to the rhombus B_4 cluster with a closed-shell singlet ground state leads to the $B_4(CO)_2$ complex, which was determined to be a σ-π diradical with an open-shell singlet ground state.[19] We now report the extension of binding of three CO ligands to B_4. The results show that the coordination of an additional CO ligand to $B_4(CO)_2$ induces a change of electronic structure from an open-shell singlet to a closed-shell singlet, demonstrating that the electronic structures of boron clusters can be effectively tuned via sequential CO ligand coordination.

Experimental and Theoretical Methods

The experiments were performed using the infrared + vacuum ultraviolet (IR + VUV) two-color ionization spectroscopy apparatus using the VUV free electron laser (VUV-FEL) described in detail previously.[20] Briefly, the neutral boron clusters were generated by laser vaporization of ^{11}B-enriched boron rod

[a] Y. Zhao,[+] S. Jiang, X. Zheng
College of Chemistry,
Zhengzhou University
Zhengzhou 450001, China
E-mail: zhxch@zzu.edu.cn
[b] Y. Zhao,[+] T. Wang,[+] C. Wang,[+] Z. Zhang,[+] H. Zheng, S. Jiang, W. Yan, Prof. Dr. H. Xie, Dr. G. Li, Prof. Dr. J. Yang, Prof. Dr. G. Wu, Prof. Dr. W. Zhang, Prof. Dr. D. Dai, Prof. Dr. H. Fan, Prof. Dr. L. Jiang, Prof. Dr. X. Yang
State Key Laboratory of Molecular Reaction Dynamics,
Dalian Institute of Chemical Physics,
Chinese Academy of Sciences
Dalian 116023, China
E-mail: gli@dicp.ac.cn
fanhj@dicp.ac.cn
ljiang@dicp.ac.cn
[c] Prof. Dr. M. Zhou
Department of Chemistry,
Collaborative Innovation Center of Chemistry for Energy Materials,
Shanghai Key Laboratory of Molecular Catalysis and Innovative Materials,
Fudan University, Shanghai 200433, China
E-mail: mfzhou@fudan.edu.cn
[d] Prof. Dr. X. Yang
Department of Chemistry,
Southern University of Science and Technology
Shenzhen 518055, China
[e] T. Wang,[+] C. Wang,[+] Z. Zhang,[+] H. Zheng, W. Yan
University of Chinese Academy of Sciences
19 A Yuquan Road, Beijing 100049, China
[+] These authors contributed equally to this work.

Supporting information for this article is available on the WWW under https://doi.org/10.1002/cphc.202200060

target with a pulsed 532 nm laser (Nd:YAG, Beamtech Optronics Co., Ltd.), and then carried into the reaction tube through a nozzle (3 mm diameter, 20 mm long) by the pulsed (Parker General Valve, Series 9) buffer gas with a 1.5 MPa backing pressure. The reaction gas (5%CO + 10%Ar + 85%He) at a backing pressure of 1.5 MPa was injected into the reaction tube by another pulsed valve (Parker General Valve, Series 9), and then react with the prepared pure boron clusters. The cluster beams passed through a 4-mm-diameter skimmer and an aperture with a 3-mm opening. Neutral clusters in the molecular beam were near-threshold ionized by the VUV-FEL pulse and mass-analyzed in the reflectron time-of-flight mass spectrometer (TOF-MS). The tunable IR light pulse was introduced at approximately 20 ns prior to the VUV-FEL pulse in a crossed manner. The heating of neutral clusters via the resonant absorption of IR photons can lead to enhanced ionization efficiency for a given cluster when its ionization potential is just above the VUV photon energy. Inasmuch as clusters with different sizes have different ionization potentials, a size-specific neutral cluster $B_m(CO)_n$ can be softly ionized without fragmentation by carefully optimizing the wavelength and pulse energy of VUV-FEL and the IR pulse energy. The TOF-MS spectral signals of a size-specific $B_m(CO)_n^+$ are not interfered with the signals of smaller and larger clusters. Mass selection of $B_m(CO)_n$ can then be achieved by monitoring the $B_m(CO)_n^+$ channel in the TOF-MS spectrum. Here, the IR spectrum of mass-selected $B_4(CO)_3$ was recorded by monitoring the enhancement in the mass spectral signal intensity of $B_4(CO)_3^+$ at the VUV-FEL wavelength of 143.00 nm as a function of IR wavelength.

The operating frequencies of the pulse valve, the 532-nm laser, and the VUV-FEL were 20 Hz, while that of the IR laser was 10 Hz. The IR spectra were obtained in the difference mode of operation (IR laser on minus IR laser off). The IR spectrum was determined by converting the measured relative enhancement of the mass spectrometric ion signal ($I(\nu)/I_0$) upon irradiation with IR light to relative absorption cross sections $\sigma(\nu)$ using $\sigma(\nu) = -\ln[I(\nu)/I_0]/P(\nu)$. The normalization with the IR laser pulse energy $P(\nu)$ accounted for the variations of $P(\nu)$ over the tuning range. Typical spectra were recorded by scanning the IR laser in steps of 2 cm^{-1} and averaging over 900 laser shots at each wavelength. IR power dependence of the signal was measured to ensure that the enhanced ionization efficiency was linear with IR photon flux.

The Dalian Coherent Light Source (DCLS) facility delivered the VUV-FEL light with a continuously tunable wavelength region between 50 and 150 nm. For recording the pulse spectral characteristic (wavelength, intensity, time profile), an online VUV spectrometer was used to monitor each single VUV-FEL pulse. The tunable IR laser beam was generated by a potassium titanyl phosphate/potassium titanyl arsenate optical parametric oscillator/amplifier system (OPO/OPA, LaserVision) pumped by an injection-seeded Nd:YAG laser (Continuum Surelite EX). This system was tunable from 700 to 7000 cm^{-1} with a line width of 1 cm^{-1}. The IR wavelength of the OPO laser output was calibrated using a commercial wavelength meter (HighFinesse GmbH, WS6-200 VIS IR).

Quantum chemical calculations were performed using the Gaussian 09 package.[21] The structures were optimized at the MN12SX/aug-cc-pVTZ level of theory. Relative energies were calculated for 0 K structures, which include the zero-point vibrational corrections. The resulting stick spectra were convoluted by a Gaussian line shape function with a 8 cm^{-1} full width at half-maximum (FWHM). The (U)CCSD(T)/6-311 + G(d) single-point energy calculations on the (U)CCSD(T)/6-31G(d) optimized structures were carried out to determine the electronic structures.

Results and Discussion

The measured IR spectrum in the carbonyl stretching frequency region for $^{11}B_4(CO)_3$ is shown in Figure 1a. The experimental IR spectrum exhibits three bands labeled as **A**, **B**, and **C**, which appear at 2111, 2169, and 2211 cm^{-1} (Table 1), respectively. These band positions feature the carbonyl stretching modes as compared to the previously reported boron carbonyl complexes.[11,18–19,22–30]

To assign the experimentally observed IR spectral features and to identify the geometric and electronic structures of $B_4(CO)_3$, quantum chemical calculations were carried out at the MN12SX/aug-cc-pVTZ level of theory. The lowest energy carbonyl structure consists of a planar rhombus B_4 core with three CO ligands terminally bonded to three B atoms, for which

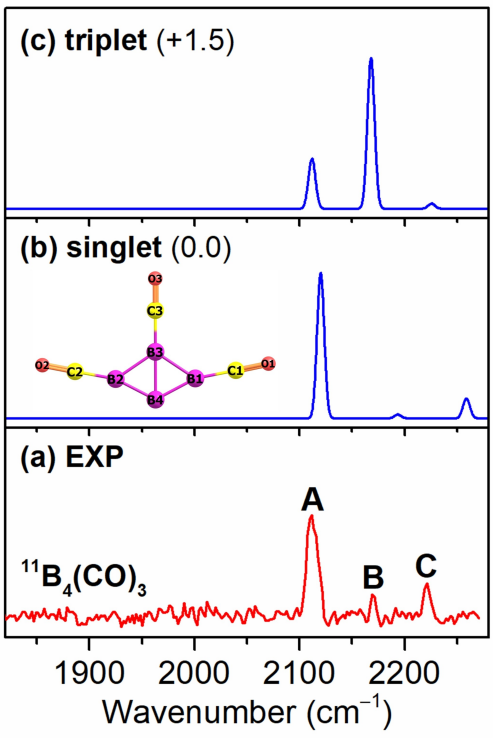

Figure 1. Experimental IR spectrum (a) and calculated IR spectra of the singlet state (b) and the triplet state (c) of $^{11}B_4(CO)_3$. The calculations were performed at the MN12SX/aug-cc-pVTZ level of theory. The structure with atom labels is embedded in the inset. Relative energies are listed in parentheses in kcal mol^{-1}.

Table 1. Comparison of the band positions (in cm^{-1}) of neutral $^{11}B_4(CO)_3$ complex measured in the present work to those of the singlet state calculated at the MN12SX/aug-cc-pVTZ level of theory (IR intensities are listed in parentheses in $km\,mol^{-1}$). The labels for the atoms are indicated in the structure in Figure 1.

Band	Exptl.	Calcd.	Assignment
A	2111	2120 (6176)	antisymmetric CO stretching mode of the C1O1 and C2O2 ligands
B	2169	2193 (174)	symmetric CO stretching mode of the C1O1 and C2O2 ligands
C	2211	2259 (852)	CO stretching mode of the C3O3 ligand

the triplet state ($^3B_2$) is 1.5 kcal/mol higher in energy than the closed-shell singlet state ($^1A_1$). The calculated IR spectra of the singlet and triplet of the lowest-energy carbonyl structure are shown in Figure 1b and 1c, respectively. Note that the IR spectrum of $B_4(CO)_3$ was measured by enhanced ionization efficiency in the linear IR absorption scheme, the experimental band intensities were proportional to the IR absorption strengths. Thus, the experimental IR spectrum resembles the linear absorption spectrum. The intensities are then more diagnostic for assigning structures than the frequencies based on conventional quantum chemical calculations, since standard computational tools give direct access to calculating linear absorption spectra, generally within the harmonic approximation, but are difficult to extend to the multiple absorption case.[31]

As shown in Figure 1, the spectrum of the singlet $B_4(CO)_3$ provides excellent match to the experimental IR spectrum. The calculated band at 2120 cm^{-1} is due to the antisymmetric stretching mode of the C1O1 and C2O2 ligands (Table 1), which is consistent with the experimental value of band **A** (2111 cm^{-1}). The calculated symmetric stretching mode of the C1O1 and C2O2 ligands at 2193 cm^{-1} is close to the experimental value of band **B** (2169 cm^{-1}). The calculated band at 2259 cm^{-1} is due to the stretching mode of the C3O3 ligand, which is in accord with the experimental value of band **C** (2211 cm^{-1}). The band positions and intensities of calculated IR spectrum of the triplet $B_4(CO)_3$ are clearly discrepant from the experimental spectrum. Thus, the observed $B_4(CO)_3$ complex can confidently be assigned to have a closed-shell electronic structure.

The identification of the singlet ground state for $B_4(CO)_3$ presents a striking difference from $B_4(CO)_2$, which was characterized to have an open-shell singlet ground state,[19] indicating that the binding of CO ligands to B_4 induces a significant change of electronic structures. To elucidate the mechanism of CO-induced tuning of the electronic structures in the B_4, $B_4(CO)_2$, and $B_4(CO)_3$ series, the (U)CCSD(T)/6-311+G(d)//(U)CCSD(T)/6-31G(d) calculations were carried out. Relative energies of the closed-shell singlet, open-shell singlet, and triplet states of B_4, $B_4(CO)_2$, and $B_4(CO)_3$ are given in Table 2. The bonding schemes of $B_4(CO)_2$ and $B_4(CO)_3$ are depicted in Figure 2.

B_4 has a close-shell singlet ground state with a valence electron configuration of $\ldots(b_{3u})^2(a_g)^2(a_g)^0(b_{1u})^0(b_{2g})^0$.[32–35] As

Table 2. Relative energies (in $kcal\,mol^{-1}$) of different electronic states of B_4, $B_4(CO)_2$, and $B_4(CO)_3$ calculated at the (U)CCSD(T)/6-311+G(d)//(U)CCSD(T)/6-31G(d) level of theory.

Cluster	Close-shell singlet	Open-shell singlet	Triplet
B_4	0.0	+4.6	+33.0
$B_4(CO)_2$	0.0	−25.2	−24.3
$B_4(CO)_3$	0.0	+2.7	+3.7

shown in Figure S3, the highest occupied molecular orbital (HOMO, a_g) is a delocalized σ bonding orbital, while the lowest unoccupied molecular orbital (LUMO, a_g) is a σ* antibonding orbital between the B3 and B4 atoms (see Figure 1 for the labels of the atoms). The LUMO+1 (b_{1u}) and LUMO+2 (b_{2g}) are the nonbonding orbitals consisting of the p_x (B1) and p_z (B2) atomic orbitals, respectively. The HOMO-1 (b_{3u}) is a fully-delocalized π bonding orbital among the four B atoms. The large HOMO-LUMO gap (207.1 kcal/mol) validates the preferred closed-shell singlet ground state. In the triplet state of B_4, one σ bonding electron of HOMO is excited to the LUMO σ* antibonding orbital (Figure S3), remarkably elevating its energy which is higher than the singlet state by 33.0 kcal/mol (Table 2).

The $B_4(CO)_2$ complex was characterized to have an open-shell $^1B_{2g}$ ground state,[19] which can be regarded as bonding between an excited state B_4 with electron configuration of $\ldots(b_{3u})^2(a_g)^1(a_g)^0(b_{1u})^0(b_{2g})^1$ and two CO ligands. As shown in Figure 2a, the vacant a_g and b_{1u} orbitals of B_4 serve as primary acceptor orbitals for donation from the 5σ lone pair orbitals of the two CO ligands, forming the fully occupied HOMO-11 and HOMO-12 σ donation bonding MOs of $B_4(CO)_2$. The singly occupied b_{2g} orbital and the HOMO (b_{3u}) interact with the 2π* antibonding MOs of the CO ligands in forming the π back-donation bonding MOs of $B_4(CO)_2$ (HOMO-1 and SOMO1 in Figure 2a). The singly occupied π backdonation bonding orbital lies very close in energy to another SOMO, which is a B3-B4 σ bonding orbital (SOMO2). Consequently, the $B_4(CO)_2$ complex is a σ-π diradical. The disjoint pattern of the σ and π orbitals, as well as the dynamic spin polarization effect leads to the violation of Hund's rule, resulting in an open-shell singlet ground state.[2,19,36]

The coordination of the third CO ligand forms the closed-shell singlet state $B_4(CO)_3$ complex, which correlates to the excited state of $B_4(CO)_2$ with the singly occupied σ electron being excited to the π orbital. In this circumstance, the σ orbital is empty and serves as the primary acceptor orbital for donation from the 5σ lone pair orbital of the third CO ligand in forming the σ donation bonding MO (HOMO-17 in Figure 2b). The π backdonation bonding orbital (LUMO in Figure 2b) formed between the antibonding 2π* orbital of the third CO ligand and the vacant orbital of $B_4(CO)_2$ (LUMO+3) lies higher in energy than the π backdonation bonding orbital involving the first two CO ligands (HOMO in Figure 2b). The closed-shell singlet state with a moderate HOMO-LUMO gap of 138.1 kcal/mol is favored over the triplet or open-shell singlet state for $B_4(CO)_3$. The triplet state is predicted to be 3.7 kcal/mol higher in energy than the closed-shell singlet state at the (U)CCSD(T)/6-311+G(d)//(U)CCSD(T)/6-31G(d) level. Since the two SOMOs of the triplet

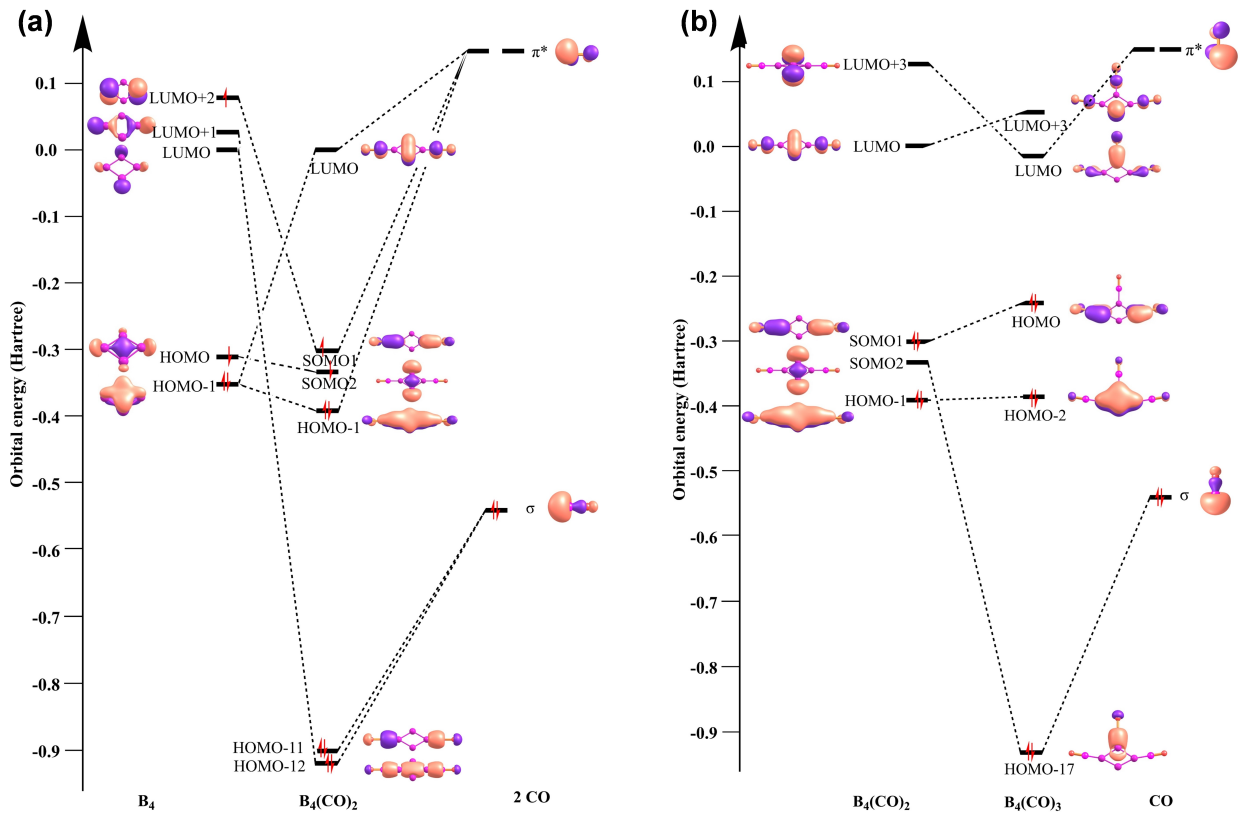

Figure 2. Bonding schemes of the open-shell singlet $B_4(CO)_2$ (a) and the close-shell singlet $B_4(CO)_3$ (b), illustrating bonding interactions between B_4, $B_4(CO)_2$, and the CO ligands. The calculations were performed at the (U)CCSD(T)/6-311+G(d)//(U)CCSD(T)/6-31G(d) level of theory.

state $B_4(CO)_3$ are not disjoint (Figure S3), the open-shell singlet state is unfavored.

It can be seen from the above bonding discussions that the electronic structure of the B_4 cluster can be tuned by the coordination of CO ligands via the OC→B_4 σ donation and B_4→CO π backdonation bonding interactions. The $B_4(CO)_2$ complex can be regarded as bonding of two CO ligands with an excited state B_4 with one of the doubly occupied HOMO σ electrons being excited to the LUMO+2 π orbital. The closed-shell singlet ground state of $B_4(CO)_3$ can be regarded as bonding between the CO ligands and an excited state of B_4 with both the HOMO σ electrons being excited to the LUMO+2 π orbital. These σ→π promotions strengthen both the OC→B_4 σ donation and B_4→CO π backdonation interactions, which result in dramatic change of the electronic structure of the B_4 core. The bare B_4 cluster with two fully delocalized σ electrons (HOMO) and two fully delocalized π electrons (HOMO-1) are double aromatic. Upon CO coordination, the delocalized σ electrons are excited to the π orbital that involves B→CO π backdonation bonding, the σ aromaticity in $B_4(CO)_2$ and $B_4(CO)_3$ is thus reduced. The aromaticities of the B_4 core in these complexes are characterized by calculating the nucleus independent chemical shift (NICS) values. The NICS values calculated at the ring centers and 1 Å above are listed in Table 3. The absolute NICS values decrease with increased CO coordination as expected.

Table 3. The nucleus independent chemical shift (NICS) values of the ground states of B_4, $B_4(CO)_2$, and $B_4(CO)_3$ calculated at the MN12SX/aug-cc-pVTZ level of theory.

Clusters	Electronic state	NICS (ring center)	NICS (1 Å above ring center)
B_4	close-shell singlet	−32.3	−7.8
$B_4(CO)_2$	open-shell singlet	−17.4	−9.9
$B_4(CO)_3$	close-shell singlet	−11.6	0.4

Conclusions

Neutral boron carbonyl complexes were generated in the gas phase. The $B_4(CO)_3$ complex was characterized by infrared+vacuum ultraviolet (IR+VUV) two-color ionization spectroscopy and quantum chemical calculations to have a closed-shell singlet ground state with planar C_{2v} structure with the three CO ligands terminally coordinated to a rhombus B_4 core. Bonding analyses on $B_4(CO)_3$ as well as the previously reported B_4 and $B_4(CO)_2$ indicate that the electronic structure of rhombus tetraboron cluster changes from a close-shell singlet to an open-shell singlet in $B_4(CO)_2$ and to a close-shell singlet in $B_4(CO)_3$, demonstrating that the electronic structures of boron clusters can be effectively tuned via sequential CO ligand coordination.

Supporting Information

Figures S1–S3 and cartesian coordinates of optimized structures.

Acknowledgments

The authors gratefully acknowledge the Dalian Coherent Light Source (DCLS) and Specreation Co., Ltd. for support and assistance. This work was financially supported by the National Natural Science Foundation of China (22125303, 92061203, 92061114, 21976049, and 21688102), the Strategic Priority Research Program of Chinese Academy of Sciences (CAS) (XDB17000000), International Partnership Program of CAS (121421KYSB20170012), CAS (GJJSTD20190002), K. C. Wong Education Foundation (GJTD-2018-06), and Dalian Institute of Chemical Physics (DICP DCLS201701 and DCLS201702).

Conflict of Interest

The authors declare no conflict of interest.

Data Availability Statement

The data that support the findings of this study are available from the corresponding author upon reasonable request.

Keywords: infrared spectroscopy · bond theory · electronic structure · cluster compound · carbon monoxide

[1] R. Hoffmann, R. B. Woodward, *Science* **1970**, *167*, 825–831.
[2] W. T. Borden, H. Iwamura, J. A. Berson, *Acc. Chem. Res.* **1994**, *27*, 109–116.
[3] S. Pedersen, J. L. Herek, A. H. Zewail, *Science* **1994**, *266*, 1359–1364.
[4] H. Ishii, K. Sugiyama, E. Ito, K. Seki, *Adv. Mater.* **1999**, *11*, 605–625.
[5] W.-J. Ong, L.-L. Tan, Y. H. Ng, S.-T. Yong, S.-P. Chai, *Chem. Rev.* **2016**, *116*, 7159–7329.
[6] L. Zhao, M. Hermann, N. Holzmann, G. Frenking, *Coord. Chem. Rev.* **2017**, *344*, 163–204.
[7] Z. Sun, Q. Ye, C. Chi, J. Wu, *Chem. Soc. Rev.* **2012**, *41*, 7857–7889.
[8] J. A. Berson, *Acc. Chem. Res.* **1997**, *30*, 238–244.
[9] W.-L. Li, X. Chen, T. Jian, T.-T. Chen, J. Li, L.-S. Wang, *Nat. Chem. Rev.* **2017**, *1*, 0071.
[10] M.-A. Legare, G. Belanger-Chabot, R. D. Dewhurst, E. Welz, I. Krummenacher, B. Engels, H. Braunschweig, *Science* **2018**, *359*, 896–899.
[11] J. Y. Jin, M. F. Zhou, *Dalton Trans.* **2018**, *47*, 17192–17197.
[12] M.-A. Legare, C. Pranckevicius, H. Braunschweig, *Chem. Rev.* **2019**, *119*, 8231–8261.
[13] B. Yoon, H. Hakkinen, U. Landman, A. S. Worz, J. M. Antonietti, S. Abbet, K. Judai, U. Heiz, *Science* **2005**, *307*, 403–407.
[14] B. K. Min, C. M. Friend, *Chem. Rev.* **2007**, *107*, 2709–2724.
[15] H. J. Freund, G. Meijer, M. Scheffler, R. Schlogl, M. Wolf, *Angew. Chem. Int. Ed.* **2011**, *50*, 10064–10094; *Angew. Chem.* **2011**, *123*, 10242–10275.
[16] X. Wu, L. L. Zhao, J. Y. Jin, S. Pan, W. Li, X. Y. Jin, G. J. Wang, M. F. Zhou, G. Frenking, *Science* **2018**, *361*, 912–916.
[17] L. B. Knight, B. W. Gregory, S. T. Cobranchi, D. Feller, E. R. Davidson, *J. Am. Chem. Soc.* **1987**, *109*, 3521–3525.
[18] M. F. Zhou, N. Tsumori, Z. H. Li, K. N. Fan, L. Andrews, Q. Xu, *J. Am. Chem. Soc.* **2002**, *124*, 12936–12937.
[19] M. F. Zhou, Q. Xu, Z. X. Wang, P. V. Schleyer, *J. Am. Chem. Soc.* **2002**, *124*, 14854–14855.
[20] G. Li, C. Wang, Q. M. Li, H. J. Zheng, T. T. Wang, Y. Yu, M. Z. Su, D. Yang, L. Shi, J. Y. Yang, Z. G. He, H. Xie, H. J. Fan, W. Q. Zhang, D. X. Dai, G. R. Wu, X. M. Yang, L. Jiang, *Rev. Sci. Instrum.* **2020**, *91*, 034103.
[21] M. J. Frisch, G. W. Trucks, H. B. Schlegel, G. E. Scuseria, M. A. Robb, J. R. Cheeseman, G. Scalmani, V. Barone, B. Mennucci, G. A. Petersson, H. Nakatsuji, M. Caricato, X. Li, H. P. Hratchian, A. F. Izmaylov, J. Bloino, G. Zheng, J. L. Sonnenberg, M. Hada, M. Ehara, K. Toyota, R. Fukuda, J. Hasegawa, M. Ishida, T. Nakajima, Y. Honda, O. Kitao, H. Nakai, T. Vreven, J. A. Montgomery Jr., J. E. Peralta, F. Ogliaro, M. J. Bearpark, J. Heyd, E. N. Brothers, K. N. Kudin, V. N. Staroverov, R. Kobayashi, J. Normand, K. Raghavachari, A. P. Rendell, J. C. Burant, S. S. Iyengar, J. Tomasi, M. Cossi, N. Rega, N. J. Millam, M. Klene, J. E. Knox, J. B. Cross, V. Bakken, C. Adamo, J. Jaramillo, R. Gomperts, R. E. Stratmann, O. Yazyev, A. J. Austin, R. Cammi, C. Pomelli, J. W. Ochterski, R. L. Martin, K. Morokuma, V. G. Zakrzewski, G. A. Voth, P. Salvador, J. J. Dannenberg, S. Dapprich, A. D. Daniels, O. Farkas, J. B. Foresman, J. V. Ortiz, J. Cioslowski, D. J. Fox, Gaussian, Inc., Wallingford, CT, USA, **2013**.
[22] Y. M. Hamrick, R. J. Vanzee, J. T. Godbout, W. Weltner, W. J. Lauderdale, J. F. Stanton, R. J. Bartlett, *J. Phys. Chem.* **1991**, *95*, 2840–2844.
[23] T. R. Burkholder, L. Andrews, *J. Phys. Chem.* **1992**, *96*, 10195–10201.
[24] M. F. Zhou, N. Tsumori, L. Andrews, Q. Xu, *J. Phys. Chem. A* **2003**, *107*, 2458–2463.
[25] M. F. Zhou, Z. X. Wang, P. V. Schleyer, Q. Xu, *ChemPhysChem* **2003**, *4*, 763–766.
[26] M. F. Zhou, L. Jiang, Q. Xu, *Chem. Eur. J.* **2004**, *10*, 5817–5822.
[27] Q. Zhang, W.-L. Li, C.-Q. Xu, M. Chen, M. Zhou, J. Li, D. M. Andrada, G. Frenking, *Angew. Chem. Int. Ed.* **2015**, *54*, 11078–11083; *Angew. Chem.* **2015**, *127*, 11230–11235.
[28] J. Jin, G. Wang, M. Zhou, D. M. Andrada, M. Hermann, G. Frenking, *Angew. Chem. Int. Ed.* **2016**, *55*, 2078–2082; *Angew. Chem.* **2016**, *128*, 2118–2122.
[29] J. Y. Jin, G. J. Wang, M. F. Zhou, *Chin. J. Chem. Phys.* **2016**, *29*, 47–52.
[30] J. Y. Jin, G. J. Wang, M. F. Zhou, *J. Phys. Chem. A* **2018**, *122*, 2688–2694.
[31] K. R. Asmis, D. M. Neumark, *Acc. Chem. Res.* **2012**, *45*, 43–52.
[32] I. Boustani, *Phys. Rev. B* **1997**, *55*, 16426–16438.
[33] H. J. Zhai, L. S. Wang, A. N. Alexandrova, A. I. Boldyrev, *J. Phys. Chem. A* **2003**, *107*, 9319–9328.
[34] R. Linguerri, I. Navizet, P. Rosmus, S. Carter, J. P. Maier, *J. Chem. Phys.* **2005**, *122*, 034301.
[35] E. M. I. Moreira, B. G. A. Brito, G. Q. Hai, L. Candido, *Chem. Phys. Lett.* **2020**, *754*, 137636.
[36] J. A. Berson, *Science* **1994**, *266*, 1338–1339.

Manuscript received: January 25, 2022
Revised manuscript received: February 21, 2022
Version of record online: March 16, 2022